Individual charge changing fragmentation cross sections of relativistic nuclei in hydrogen, helium, and carbon targets

W. R. Webber, J. C. Kish, and D. A. Schrier
Space Science Center, University of New Hampshire, Durham, New Hampshire 03824
(Received 19 December 1988)

In this paper we describe individual elemental cross sections. Over 100 of these cross sections have been measured by studying the fragmentation of beams of 12 charges ranging from ^{12}C to ^{58}Ni in hydrogen, helium, and carbon targets. The energies of the beams ranged from ~300 to 1700 MeV/nucleon. The relative cross sections in hydrogen, helium, and carbon targets are examined as a function of both beam charge and energy. Limits are placed on the energy region in which the concept of factorization or scaling of cross sections for different beam charges and targets applies. The approach of these elemental cross sections to the asymptotic high-energy values is examined as a function of the beam charge and the charge change. The systematics of the energy dependence of these cross sections is also described in terms of the beam charge and the charge change. Another important systematic in our data is a regular decrease in the elemental cross sections into a particular charge, Z_f, with increasing charge change at a constant energy. It is found that this regular behavior of the cross sections follows a simple exponential law in the charge change, $Z_B - Z_f$. This has important implications for constructing an empirical formula to describe these cross sections, as well as having theoretical implications.

I. INTRODUCTION

This is the second in a series of papers dealing with the cross sections measured using ^{12}C, ^{14}N, ^{15}O, ^{20}Ne, ^{24}Mg, ^{27}Al, ^{28}Si, ^{32}S, ^{40}Ar, ^{40}Ca, ^{56}Fe, and ^{58}Ni beams with energies between 300 and 1700 MeV/nucleon incident on hydrogen (CH_2), helium, and carbon targets at the Lawrence Berkeley Laboratory Bevalac. In this paper we will discuss the individual elemental charge changing cross sections. This work is part of a systematic study of the individual elemental and isotopic cross sections for hydrogen and helium targets appropriate to the interpretation of the interstellar production of secondary fragments during cosmic-ray propagation in the galaxy, and so to determine the source elemental and isotopic components of cosmic rays. At the same time it should be noted that the basic systematics of these individual elemental cross sections as a function of the incident charge, energy, and target are an important input for understanding the nuclear physics involved in these peripheral collisions.

The basic details of these runs at the Bevalac with a total of 42 separate beams of the 12 charges listed earlier, are described in paper I.[1] In this paper we will discuss the individual elemental cross sections obtained. These will be compared with other measurements of individual elemental cross sections that have recently been measured, mainly at the Bevalac, which for many years was the only source of energetic heavy ions available in the world. The large volume of data from these new studies allows us to study the systematics of the cross sections as a function of charge, energy, and target in unprecedented detail, and this new data will be compared with previous semiempirical models used to describe this fragmentation.

II. THE EXPERIMENT AND THE MEASUREMENT TECHNIQUES

The general properties of the experimental set up have been described in paper I.[1] An outline drawing of the telescope is shown in Fig. 1 of paper I. The telescope basically consists of three separate modules; a charge identification module, an isotope identification module, and a fragment module. For the study here, only the charge identification module was used. Individual secondary fragment charges were identified from cross plots of the various scintillators and the Cerenkov counter. The targets used and the procedures for alternating the targets with the no target run are described in paper I.[1]

III. DATA ANALYSIS AND THE DETERMINATION OF THE PARTIAL CHARGE CHANGING CROSS SECTIONS

The individual charge fragments are identified from cross plots of the $S1$–$S2$ and $S2$–$S3$ scintillators, an example of which is shown in Fig. 1 for a CH_2 target using an ^{27}Al beam at 550 MeV/nucleon. The individual fragments produced in the target can be clearly identified lying along the diagonal in these plots. Also seen in this figure are the interactions occurring in the $S1$ scintillator, lying along vertical bands, together with fragments from secondary interactions in the scintillators and in the beam. For fragment charges Z_f the effective charge resolution deteriorates because of the fact that there are a larger number of fragmentation modes possible as the charge difference, $Z_i - Z_f$, increases. In general we cannot obtain useful individual elemental fragmentation cross sections when $Z_f \leq 0.5 Z_i$ because of this problem. A close examination of the charge peaks also shows that

they are not exactly Z_f^2 dependent as expected for individual fragments, but instead follow more closely a Z_{eff}^2 dependence, where Z_{eff}^2 is given by the sum of the squares of the charge of the principal fragment plus all of the remaining fragment charges [see also Figs. 2(a)–(c)], which are mainly identified as $Z=1$ or 2 (see Webber and Brautigam[2]). Note also that there is a broad peak corresponding to a low value of Z_{eff}. This peak is present in all runs, but is strongly energy dependent and is due to the almost complete fragmentation of the beam nuclei. The value of Z_{eff}^2 corresponds to almost all of these fragments being protons.

It is important to note that, to determine the total interaction cross sections in this analysis for comparison with the results on the total cross sections reported in paper I, all of the secondary fragments, both at high and low Z, must be taken into account. Cross plots similar to those in Fig. 2 are constructed for all of the separate target runs for a given beam, including the no target run. In the no-target runs the number of events in the diagonal band corresponding to the principal fragments is generally $\leq 5\%$ of the number in the target runs. The individual elemental cross sections are determined from the number of fragment nuclei produced in the target that survive through the charge measuring part of the telescope ($S1$–$S3$ coincidence). To take into account interactions occurring in the telescope and to obtain better defined charge distributions we place consistency criteria on the outputs of the $S1$–$S3$ scintillators. This consistency was chosen to be $\pm 3\sigma$ for each charge in each scintillator for $Z_f > 0.5Z_i$, becoming broader for the lower Z_f fragments that cannot be as easily identified. It was verified that the section criteria that were used removed a negligible fraction of the noninteracting fragments, but detected and removed $\geq 95\%$ of all of the beam nuclei or principal secondary fragments that interacted in the charge module after the $S1$ counter. For events satisfying this selection criteria, charge histograms for each target were constructed including the no-target runs, which were subjected to the same criteria. In Figs. 2(a)–(c) we show examples of these charge histograms for carbon targets for incident beams of ^{16}O, ^{32}S, and ^{56}Fe nuclei. These histograms may be directly compared with those shown in Fig. 2 of paper I, which were made without the selection criteria. The raw number of events for each fragment charge for the various beams, energies, and targets are obtained from histograms such as those in Fig. 2. For this determination the number of events assigned to each charge, Z_f, is taken to be the number of events lying between $Z_f \pm 0.5$ on the histogram.

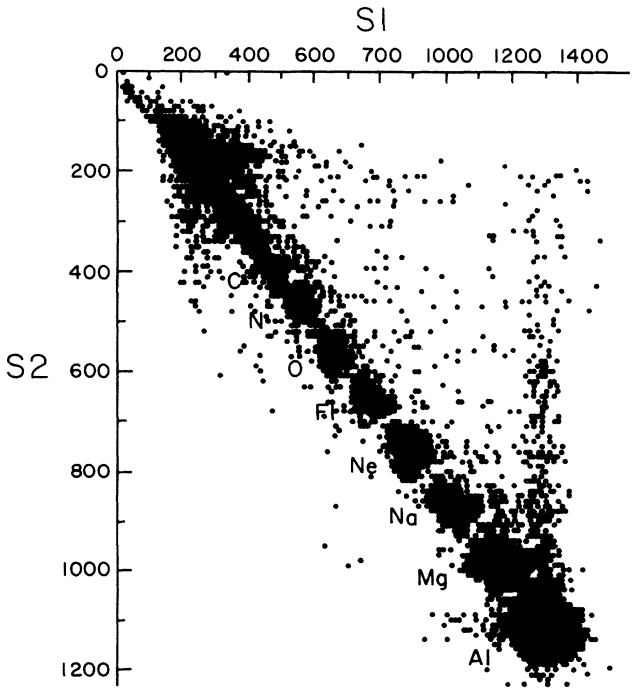

FIG. 1. Cross plot of events in $S1$ vs $S2$ counters for a 550 MeV/nucleon ^{27}Al beam incident on a CH_2 target.

These numbers have to be corrected for various effects in order to arrive at a set of numbers that can be used to derive the cross sections. For each of the targets, CH_2, C, and He, the events are first corrected for the target out, corresponding to interactions in the beam line and in $S1$. In this correction the total number of events in the no-target runs satisfying the selection criteria are normalized to the total number in the corresponding target runs, and the number of events for each fragment element in the no-target runs are then subtracted from the target runs. The second correction is for the interactions of the beam and fragment nuclei that occur in the charge module part of the telescope. This correction assumes that essentially all of the charge changing interactions occurring in the telescope are identified and removed by the $S1$–$S3$, criteria, therefore the correction to the top of the telescope is given by

$$N_{\text{obs}}(Z)=N_T(Z)\exp^{x/\lambda_{\text{tel}}(Z)} ,$$

where N_{obs} is the observed number of events of fragment charge Z_f after the selection criteria, N_T is the number emerging from the target, x is the total thickness of the various materials in the telescope, and $\lambda_{\text{tel}}(Z)$ are the interaction mean free paths of each fragment in each of the telescope materials. The mean free paths used in this calculation are obtained from

$$\lambda(Z)=\frac{m_{\text{tel}}}{\sigma_Z} ,$$

where

$$\sigma_Z=\pi r_0^2(A_T^{1/3}+A_Z^{1/3}-b)^2 ,$$

where $r_0=1.35\times 10^{-13}$ cm and, the overlap parameter b is adapted from our own total interaction cross section measurements reported in paper I.

The material in the charge defining part of the telescope ranges from ~ 0.3 of an interaction length for a ^{12}C beam to ~ 0.6 of an interaction length for a ^{56}Fe beam. When the interaction correction is made it is found that

the total number of beam charge counts, N_B, obtained from the data with selection criteria equals the total number observed directly in $S1$ from the no criteria data (as discussed in paper I) to within $\pm 1\%$.

The final correction is based on the fact that the sum of all of the fragment fractions $\sum_{Z_f} N_{if}(Z)/N_B$, must be equal for the data with selection criteria and the data without selection criteria, as is determined directly from the $S1$ distribution. This assures that the total charge changing cross sections derived from the data employing selection criteria are identical to those obtained directly from the data without selection criteria, as described in paper I. Because of multiple fragments and the difficulty of employing consistent selection criteria for $Z_f \leq 0.5Z_i$,

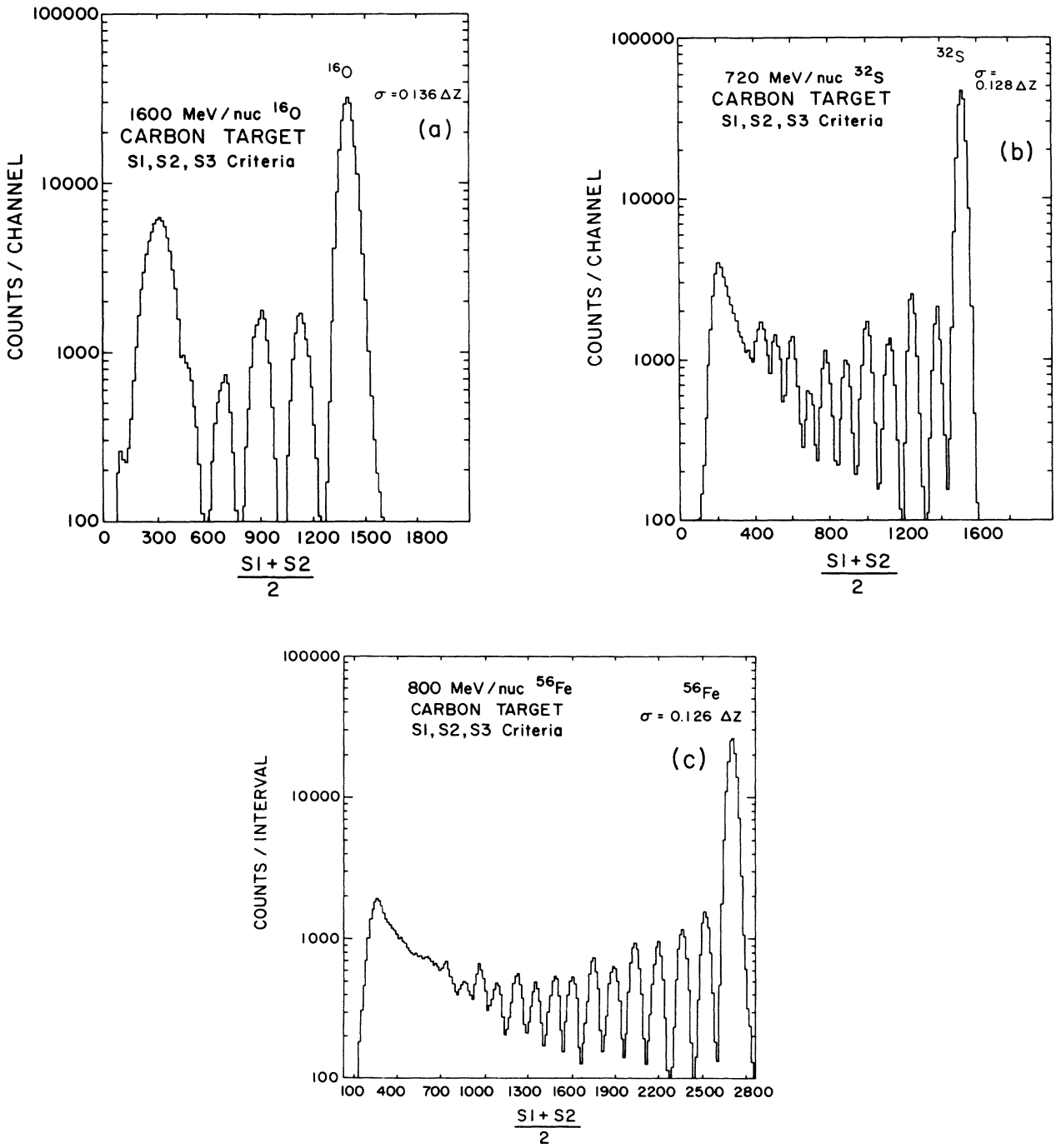

FIG. 2. (a) Distribution of events in the $S1$ and $S2$ counters subject to $S1$–$S3$ criteria for 600 MeV/nucleon ^{16}O incident on a carbon target. (b) As in (a) but for 720 MeV/nucleon ^{32}S nuclei incident on a carbon target. (c) As in (a) but for 810 MeV/nucleon ^{56}Fe nuclei incident on a carbon target.

TABLE I. Individual elemental cross sections (in mb) (Z_B=6–13). 1=carbon target, 2=hydrogen target, and 3=helium target. Errors: $A=\pm1.5\%$, $B=\pm3\%$, $C=\pm5\%$, $D=\pm10\%$, and $E=\pm20\%$.

Beam		^{11}B			^{12}C					^{14}N		^{16}O	
Energy (MeV/nucleon)		326	403	418	561	693	915	1016	1572	516	441.0	491.0	669.0
delta Z													
1	1	105.9 (*A*)	106.0 (*A*)	111.2 (*A*)	108.7 (*A*)	110.1 (*A*)	109.4 (*A*)	113.2 (*A*)	103.9 (*A*)	169.2 (*A*)	162.9 (*A*)	146.4 (*A*)	158.5 (*A*)
	2	40.1 (*C*)	43.1 (*C*)	45.2 (*C*)	53.3 (*C*)	48.8 (*C*)	51.2 (*C*)	49.8 (*C*)	50.9 (*C*)	75.0 (*C*)	74.5 (*C*)	71.0 (*C*)	70.6 (*C*)
	3				75.2 (*A*)				69.6 (*A*)	116.4 (*A*)		90.3 (*A*)	
2	1	30.1 (*B*)	29.6 (*B*)	32.1 (*B*)	30.3 (*B*)	34.9 (*B*)	33.6 (*B*)	36.8 (*B*)	35.6 (*B*)	63.1 (*B*)	160.2 (*A*)	146.2 (*A*)	159.6 (*A*)
	2	14.6 (*C*)	13.2 (*C*)	14.7 (*C*)	14.1 (*C*)	14.6 (*C*)	14.9(*C*)	16.2 (*C*)	17.4 (*C*)	27.2 (*C*)	64.5 (*C*)	66.7 (*C*)	64.8 (*C*)
	3				20.9 (*B*)					46.2 (*B*)		98.3 (*A*)	
3	1									27.9 (*B*)	60.7 (*B*)	54.7 (*B*)	56.5 (*B*)
	2									13.5 (*B*)	24.8 (*C*)	23.8 (*C*)	25.1 (*C*)
	3									24.7 (*B*)		45.4 (*B*)	
4	1										13.6 (*C*)	13.4 (*C*)	17.3 (*C*)
	2										7.0 (*D*)	8.6 (*D*)	9.2 (*D*)
	3												

Beam		^{16}O		^{20}Ne			^{23}Na		^{24}Mg				^{27}Al
Energy (MeV/nucleon)		903.0	1563	468	599	608	1057	461	309	481	739	1455	582
delta Z													
1	1	154.4 (*A*)	125.3 (*A*)	106.3 (*A*)	91.6 (*A*)	96.9 (*A*)	87.6 (*A*)	132.3 (*B*)	147.8 (*A*)	124.3 (*A*)	116.1 (*A*)	116.4 (*A*)	182.1 (*A*)
	2	68.6 (*C*)	64.9 (*C*)	44.6 (*C*)	48.7 (*C*)	44.8 (*C*)	47.1 (*C*)	80.9 (*C*)	80.5 (*C*)	85.4 (*C*)	82.2 (*C*)	80.7 (*C*)	112.1 (*C*)
	3		80.3 (*A*)										120.3 (*A*)
2	1	152.9 (*A*)	123.2 (*A*)	181.0 (*A*)	150.6 (*A*)	159.5 (*A*)	140.1 (*A*)	62.1 (*B*)	133.0 (*A*)	111.0 (*A*)	102.2 (*A*)	101.5 (*A*)	95.6 (*A*)
	2	61.7 (*C*)	64.8 (*C*)	81.6 (*C*)	74.6 (*C*)	67.7 (*C*)	76.3 (*C*)	35.7 (*C*)	64.8 (*C*)	64.1 (*C*)	63.2 (*C*)	62.7 (*C*)	51.3 (*C*)
	3		89.5 (*A*)										71.9 (*A*)
3	1	52.4 (*B*)	46.6 (*B*)	134.5 (*B*)	111.1 (*B*)	118.8 (*B*)	103.0 (*B*)	106.1 (*B*)	58.1 (*B*)	56.3 (*B*)	48.7 (*B*)	48.0 (*B*)	89.4 (*A*)
	2	22.8 (*C*)	26.4 (*C*)	61.2 (*C*)	60.1 (*C*)	62.3 (*C*)	56.7 (*C*)	61.8 (*C*)	23.2 (*C*)	28.4 (*C*)	29.1 (*C*)	31.7 (*C*)	50.1 (*C*)
	3		4.01 (*B*)										71.7 (*A*)
4	1	20.3 (*C*)	18.2 (*C*)	135.1 (*B*)	125.9 (*B*)	120.2 (*B*)	119.8 (*B*)	89.3 (*B*)	136.6 (*A*)	119.7 (*A*)	103.5 (*A*)	106.5 (*A*)	37.6 (*C*)
	2	10.5 (*D*)	12.8 (*D*)	56.6 (*C*)	59.1 (*C*)	56.5 (*C*)	62.4 (*C*)	40.7 (*C*)	58.4 (*C*)	59.6 (*C*)	58.6 (*C*)	60.1 (*C*)	16.9 (*D*)
	3												33.6 (*C*)
5	1			53.7 (*C*)	52.6 (*C*)	53.6 (*C*)	57.2 (*C*)	101.2 (*B*)	89.8 (*B*)	89.4 (*B*)	75.9 (*B*)	73.8 (*B*)	81.5 (*B*)
	2			13.1 (*D*)	14.3 (*D*)	17.6 (*D*)	22.1 (*D*)	47.8 (*C*)	33.7 (*C*)	35.6 (*C*)	37.0 (*C*)	41.1 (*C*)	44.3 (*C*)
	3												58.6 (*D*)
6	1								114.3 (*B*)	120.4 (*B*)	108.6 (*B*)	106.6 (*B*)	60.2 (*B*)

TABLE I. (*Continued*).

Beam Energy (MeV/nucleon)		^{16}O			^{20}Ne		^{23}Na		^{24}Mg			^{27}Al	
		903.0	1563	468	599	608	1057	461	309	481	739	1455	582
	2								38.1 (*C*)	40.4 (*C*)	43.2 (*C*)	46.6 (*C*)	24.2 (*D*)
	3												46.2 (*D*)
7	1								39.8 (*C*)	48.1 (*C*)	45.6 (*D*)	48.6 (*C*)	74.1 (*C*)
	2								11.5 (*D*)	13.3 (*D*)	15.8 (*D*)	24.9 (*D*)	29.5 (*D*)
	3												66.1 (*C*)
8	1												37.6 (*D*)
	2												8.8 (*E*)

it is necessary to renormalize the sum $\sum_{Z_f} N_{if}(Z)$ for the data with selection criteria by a small factor that depends on the beam, energy, and target but is generally in the range 1.05–1.15. To the extent that the charge selection criteria remove all the interacting events as verified by the fact that the value of N_B is essentially the same as determined from $S1$ alone, as is determined after selection criteria are applied along with the interaction correction, we have no evidence of any charge dependent effects in the selection procedure.

The fully corrected numbers of events for each fragment charge are then expressed as a fraction of the number of beam charge events exiting the target. These fractions form the basic data for determining the individual elemental cross sections. If the targets had been very thin then the cross sections for the production of a fragment of charge Z_f, from the beam charge, Z_B, $\sigma_f(Z)$, could be found from

$$\sigma_f(Z)/\sigma_{\text{tot}} = N_{fT}(Z) \Big/ \sum_{Z_f} N_{fT}(Z) \ .$$

However, the targets used were all between 0.4 and 0.6 of the beam charge mean free path, hence some of the fragments produced will have secondary interactions before they leave the target (in effect, a thick target). In order to correct for these secondary interactions a one-dimensional diffusion equation of the form

$$\frac{dN_{Zf}(x)}{dx} = -\frac{\sigma_{Zf} N_Z(x)}{m_{\text{tar}}} + \sum_{Z>Z_f} \frac{\sigma_{ZZ_f}}{m_{\text{tar}}} N_Z(x)$$

was used, where $N_{Zf}(x)$ is the abundance of fragment with charge Z_f at depth x in the target, σ_{Zf} is the total charge changing cross section for this charge, σ_{ZZ_f} is the partial charge changing cross section from charge Z to charge Z_f, and $N_Z(x)$ is the abundance of the charge $Z > Z_f$. In this equation it is assumed that energy loss in the target is not important and the derived cross sections are appropriate to the average interaction energy in the target.

In this calculation the measured charge fraction of each fragment charge relative to the beam charge is the input and the program calculates the cross section of the beam charge into that fragment charge. This program requires estimates of all of the relevant secondary cross sections as well. The initial estimates of these secondary cross sections were based on the Tsao and Silberberg[3] semiempirical formulation. Later we developed a semiempirical formulation based on our data (Webber[4]) and this was used to estimate the secondary cross sections in a self-consistent manner. The importance of the production of a given Z_f from secondary interactions in the target increases as $Z_B - Z_f$ increases. For $Z_f = 0.5Z_B$, typically $\sim 30\%$ of this fragment is produced by secondary interactions so that assuming, for example, a $\pm 10\%$ error in the secondary cross sections[4] leads to an error $\sim \pm 3\%$ in the derived cross sections of the beam charge

TABLE II. Individual elemental cross-sections (in mb) ($Z_B = 14$–20). 1 = carbon target, 2 = hydrogen target, and 3 = helium target. Errors: $A = \pm 1.5\%$, $B = \pm 3\%$, $C = \pm 5\%$, $D = \pm 10\%$, and $E = \pm 20\%$.

Beam Energy (MeV/nucleon)		^{28}Si 503	^{28}Si 770	^{28}Si 1296	^{32}S 649	^{32}S 1149	^{40}Ar 521	^{40}Ar 792	^{40}Ca 672
delta Z									
1	1	130.2 (*A*)	157.4 (*A*)	160.1 (*A*)	127.2 (*A*)	121.3 (*A*)	180.7 (*A*)	186.7 (*A*)	104.6 (*A*)
	2	86.6 (*C*)	82.9 (*C*)	77.7 (*C*)	79.6 (*C*)	71.2 (*C*)	134.5 (*C*)	124.6 (*C*)	67.1 (*C*)
	3								
2	1	140.9 (*A*)	162.7 (*A*)	164.2 (*A*)	152.1 (*A*)	150.9 (*A*)	121.8 (*A*)	124.7 (*A*)	140.4 (*A*)
	2	83.5 (*C*)	76.0 (*C*)	75.1 (*C*)	103.8 (*C*)	85.8 (*C*)	104.3 (*C*)	87.6 (*C*)	92.7 (*C*)
	3								
3	1	68.4 (*B*)	64.4 (*B*)	52.3 (*B*)	88.8 (*B*)	83.9 (*B*)	93.3 (*B*)	87.9 (*B*)	79.3 (*B*)
	2	37.3 (*C*)	36.5 (*C*)	37.7 (*C*)	53.1 (*C*)	46.0 (*C*)	74.0 (*C*)	65.6 (*C*)	55.4 (*C*)
	3								
4	1	72.2 (*B*)	62.5 (*B*)	52.8 (*B*)	103.8 (*B*)	101.3 (*B*)	97.1 (*B*)	93.1 (*B*)	112.8 (*B*)
	2	36.0 (*C*)	35.8 (*C*)	39.0 (*C*)	69.7 (*C*)	56.7 (*C*)	75.6 (*C*)	73.6 (*C*)	78.8 (*C*)
	3								
5	1	31.2 (*C*)	30.2 (*C*)	25.2 (*C*)	58.1 (*C*)	55.3 (*C*)	69.3 (*C*)	62.0 (*C*)	57.7 (*C*)
	2	15.6 (*D*)	15.8 (*D*)	17.8 (*D*)	33.6 (*D*)	29.6 (*D*)	46.6 (*D*)	45.6 (*D*)	44.0 (*D*)
	3								
6	1	68.3 (*B*)	65.3 (*B*)	53.4 (*B*)	60.3 (*B*)	58.2 (*B*)	65.6 (*B*)	58.8 (*B*)	105.7 (*B*)
	2	35.5 (*C*)	34.6 (*C*)	36.3 (*C*)	29.5 (*C*)	28.5 (*C*)	37.8 (*C*)	41.7 (*C*)	68.5 (*C*)
	3								
7	1	40.3 (*C*)	48.3 (*C*)	43.9 (*C*)	26.3 (*C*)	20.7 (*C*)	44.6 (*C*)	44.1 (*C*)	53.8 (*C*)
	2	16.1 (*D*)	18.0 (*D*)	20.2 (*D*)	13.9 (*D*)	13.2 (*D*)	20.3 (*D*)	22.1 (*D*)	31.4 (*D*)
	3								
8	1	72.5 (*C*)	74.2 (*C*)	71.2 (*C*)	65.3 (*B*)	56.3 (*B*)	37.5 (*C*)	40.7 (*C*)	68.3 (*C*)
	2	22.8 (*D*)	24.5 (*D*)	31.5 (*D*)	22.8 (*C*)	33.7 (*C*)	10.2 (*D*)	15.6 (*D*)	32.9 (*D*)
	3								
9	1				63.1 (*B*)	52.7 (*B*)	31.7 (*D*)	25.1 (*D*)	37.9 (*D*)
	2				16.3 (*C*)	19.2 (*C*)	5.6 (*E*)	12.2 (*E*)	16.4 (*E*)
	3								
10	1				71.9 (*C*)	78.3 (*C*)	50.6 (*D*)	47.5 (*D*)	35.4 (*D*)
	2				21.6 (*D*)	33.3 (*D*)	6.1 (*E*)	10.3 (*E*)	12.6 (*E*)
	3								

TABLE III. Individual elemental cross sections (in mb) ($Z_B=26$). 1=carbon target, 2=hydroge target, and 3=helium target. Errors: $A=\pm1.5\%$, $B=\pm3\%$, $C=\pm5\%$, $D=\pm10\%$, and $E=\pm20\%$.

Beam Energy (MeV/nucleon)		^{56}Fe									
		330	434	520	662	724	944	1086	1409	1512	1615
delta Z											
1	1	244.3 (*B*)	223.8 (*A*)	206.2 (*A*)	191.6 (*A*)	166.5 (*A*)	177.8 (*A*)	157.7 (*A*)	162.2 (*A*)	160.2 (*A*)	150.6 (*A*)
	2	156.3 (*C*)	140.2 (*B*)	142.6 (*C*)	131.0 (*B*)	123.2 (*B*)	115.0 (*B*)	110.1 (*B*)	111.5 (*B*)	109.8 (*B*)	109.4 (*B*)
	3		160.5 (*A*)			135.9 (*A*)				129.4 (*A*)	
2	1	182.7 (*B*)	175.1 (*A*)	163.4 (*A*)	163.2 (*A*)	130.9 (*A*)	130.4 (*A*)	113.3 (*A*)	106.8 (*A*)	102.4 (*A*)	99.7 (*A*)
	2	141.5 (*C*)	128.3 (*B*)	121.1 (*B*)	109.0 (*B*)	98.0 (*B*)	97.0 (*B*)	86.6 (*B*)	88.6 (*B*)	184.4 (*B*)	78.8 (*B*)
	3		130.9 (*A*)			109.1 (*A*)				94.5 (*A*)	
3	1	121.1 (*B*)	116.1 (*B*)	115.2 (*B*)	114.3 (*B*)	91.5 (*B*)	86.7 (*B*)	77.9 (*B*)	73.5 (*B*)	79.5 (*B*)	74.7 (*B*)
	2	84.8 (*C*)	89.9 (*C*)	89.2 (*C*)	77.5 (*C*)	73.8 (*C*)	73.3 (*C*)	66.4 (*C*)	64.0 (*C*)	63.7 (*C*)	60.7(*C*)
	3		92.5 (*B*)			77.4 (*B*)				66.5 (*B*)	
4	1	110.7 (*B*)	116.0 (*B*)	112.3 (*B*)	105.3 (*B*)	87.7 (*B*)	85.3 (*B*)	76.4 (*B*)	72.7 (*B*)	79.3 (*B*)	73.7 (*B*)
	2	86.8 (*C*)	85.0 (*C*)	86.6 (*C*)	73.2 (*C*)	73.8 (*C*)	70.7 (*C*)	70.1 (*C*)	61.8 (*C*)	62.0 (*C*)	59.4 (*C*)
	3		90.7 (*B*)			74.9 (*B*)				63.7 (*B*)	
5	1	89.2 (*B*)	79.8 (*B*)	76.7 (*B*)	68.9 (*B*)	66.1 (*B*)	66.7 (*B*)	56.4 (*B*)	53.3 (*B*)	57.1 (*B*)	54.5 (*B*)
	2	51.8 (*C*)	58.2 (*C*)	59.8 (*C*)	59.4 (*C*)	55.9 (*C*)	55.2 (*C*)	51.5 (*C*)	47.4 (*C*)	44.1 (*C*)	47.3 (*C*)
	3		67.8 (*B*)			57.3 (*B*)				50.7 (*B*)	
6	1	79.6 (*B*)	73.9 (*B*)	71.3 (*B*)	69.6 (*B*)	62.0 (*B*)	60.2 (*B*)	57.8 (*B*)	56.9 (*B*)	55.7 (*B*)	54.8 (*B*)
	2	42.1 (*C*)	46.3 (*C*)	55.1 (*C*)	52.4 (*C*)	51.5 (*C*)	56.3 (*C*)	51.5 (*C*)	49.6 (*C*)	43.9 (*C*)	48.8 (*C*)
	3		68.3 (*B*)			57.5 (*B*)				49.9 (*B*)	
7	1	51.6 (*C*)	52.3 (*C*)	51.8 (*C*)	49.8 (*C*)	45.4 (*C*)	41.4 (*C*)	40.7 (*C*)	40.8 (*C*)	41.3 (*C*)	38.4 (*C*)
	2	18.8 (*D*)	21.3 (*D*)	26.9 (*D*)	29.4 (*D*)	30.2 9*D*)	37.6 (*D*)	35.8 (*D*)	32.1 (*D*)	33.2 (*D*)	31.7 (*D*)
	3		47.0 (*C*)			44.4 (*C*)				39.8 *C*()	
8	1	44.4 (*C*)	48.2 (*C*)	52.8 (*C*)	52.9 (*D*)	47.8 (*C*)	43.4 (*C*)	42.1 (*C*)	40.3 (*C*)	39.5 (*C*)	36.6 (*C*)
	2	12.4 (*D*)	19.6 (*D*)	23.8 (*D*)	27.2 (*D*)	27.3 (*D*)	38.0 (*D*)	33.5 (*D*)	30.7 (*D*)	33.0 (*D*)	30.7 (*D*)
	3		42.9 (*C*)			42.1 (*C*)				38.8 (*C*)	
9	1	38.2 (*C*)	39.5 (*C*)	40.6 (*C*)	41.8 (*C*)	35.5 (*C*)	37.6 (*C*)	35.4 (*C*)	35.7 (*C*)	33.6 (*C*)	33.7 (*C*)
	2	4.2 (*E*)	6.8 (*E*)	15.6 (*D*)	17.2 (*D*)	18.6 (*D*)	22.6 (*D*)	22.4 (*D*)	21.3 (*D*)	23.5 (*D*)	21.9 (*D*)
	3		33.2 (*C*)			33.1 (*C*)				31.6 (*C*)	
10	1	42.4 (*C*)	44.3 (*C*)	41.7 (*C*)	45.8 (*C*)	39.6 (*C*)	43.9 (*C*)	40.6 (*C*)	42.3 (*C*)	39.7 (*C*)	36.0 (*C*)
	2	6.8 (*E*)	8.0 (*E*)	17.5 (*D*)	18.3 (*D*)	18.5 (*D*)	29.6 (*D*)	27.4 (*D*)	26.2 (*D*)	26.8 (*D*)	27.1 (*D*)
	3		37.6 (*C*)			37.9 (*C*)				35.0 (*C*)	
11	1		24.89 (*D*)	29.5 (*D*)	32.0 (*D*)	29.3 (*D*)	29.8 (*D*)	28.5 (*D*)	34.6 (*D*)	31.1 (*D*)	28.1 (*D*)
	2		4.0 (*E*)	5.8 (*E*)	8.4 (*E*)	8.8 (*E*)	14.2 (*E*)	15.0 (*E*)	16.1 (*E*)	17.6 (*E*)	18.3 (*E*)
	3		22.7 (*D*)			24.4 (*D*)				25.7 (*D*)	
12	1		45.7 (*D*)	48.6 (*D*)	48.3 (*D*)	44.3 (*D*)	43.7 (*D*)	44.1 (*D*)	42.3 (*D*)	40.9 (*D*)	38.3 (*D*)
	2		6.9 (*E*)	8.8 (*E*)	10.1 (*E*)	11.9 (*E*)	19.6 (*E*)	19.5 (*E*)	18.9 (*E*)	25.6 (*E*)	23.2 (*E*)
	3		39.1 (*D*)			40.6 (*D*)				41.3 (*D*)	
13	1							27.2 (*D*)	28.4 (*D*)	28.5 (*D*)	25.7 (*D*)
	2							12.8 (*E*)	13.4 (*E*)	15.0 (*E*)	13.1 (*E*)

TABLE III. (*Continued*).

	Beam Energy (MeV/nucleon)	^{56}Fe 330	434	520	662	724	944	1086	1409	1512	1615
	3									28.4 (*D*)	
14	1							35.9 (*D*)	33.6 (*D*)	34.2 (*D*)	28.9 (*D*)
	2							6.8 (*E*)	10.9 (*E*)	14.2 (*E*)	12.2 (*E*)
	3									32.1 (*D*)	

into that principal fragment charge.

The derived charge changing cross sections in mb for C, He, and H targets for the various beams and mean target energies are shown in Tables I–III. In these tables we have emphasized the derived H cross sections, since they are of principal interest for the astrophysical problems. The measured CH_2 cross sections are simply the carbon cross sections times twice the hydrogen cross sections. A few remarks about the uncertainties in the cross sections are in order. These uncertainties may be either charge dependent or systematic affecting all charges approximately equally. Charge dependent uncertainties include:

(1) Statistical. The raw number of secondary fragments of a given charge is generally in the range 2 000–20 000, leading to statistical errors between 0.7–2.2 %. For hydrogen, the statistical errors are on the differences in the numbers of events between CH_2 and C targets. This leads to errors ~ 1.5 times those for the individual targets.

(2) No target correction. This correction ranges from a high $\sim 12\%$ for fragments with $\Delta Z = 1$ in carbon targets to a low $\sim 5\%$. This correction is straightforward and can be made to an accuracy $\leq 10\%$ leading to an overall uncertainty $\leq 1.2\%$.

(3) Correction to the top of the telescope. This correction due to interactions in the telescope is in the range 30–50 % and requires an understanding of the total interaction cross sections in the various telescope materials. This correction can be made to an estimated accuracy $< +3\%$, leading to an overall uncertainty of $50\% \times 3\% = \leq 1.5\%$.

(4) Secondary fragmentation in the target. As noted before, this correction ranges from a few percent for fragments with $\Delta Z = 1$ to a maximum $\sim 30\%$ for fragments where $Z_f \sim 0.5 Z_B$. Assuming the secondary cross sections are known to an accuracy of $\pm 10\%$ this correction can be made to a maximum uncertainty of 3% for charges with $Z_f \sim 0.5 Z_B$ and is $\lesssim 1\%$ for small ΔZ.

(5) There is also a "background" correction only for fragments with $0.5 Z_B \leq Z_f < 0.6 Z_B$, because of the fact that combinations of lower Z fragments may directly simulate a fragment with this Z_f. This effect may be seen in Figs. 2(b) and (c). This correction may be estimated from the uniform falloff of the background distribution of lower Z pulse heights and can amount to a correction for 20% for the lowest Z fragments analyzed. The uncertainty in this correction is estimated to be $\sim \pm 25\%$, giving an overall uncertainty $\leq 5\%$.

The largest systematic uncertainty is the correction for selection criteria effects and the renormalization effect. As described earlier, this can range from ~ 5 to ~ 15 % for different beams, targets, and energies. It is difficult to evaluate the uncertainty in this correction but various simple tests on the data suggest that overall this should introduce an uncertainty no larger than $\pm 3\%$.

Overall then, the absolute accuracy on the derived cross sections, assuming the charge dependent uncertainties add in quadrature, is $\lesssim 3.6\%$ for fragment charges where $Z_f \geq 0.75 Z_B$, increasing to ~ 8–10 % for fragment charges where $Z_f \sim 0.5 Z_B$. The uncertainties for hydrogen targets are about $1.5x$ the above.

IV. SYSTEMATICS OF THE CROSS SECTIONS AND A COMPARISON WITH OTHER MEASUREMENTS

The cross section data set we have obtained is perhaps the most comprehensive available for nuclei with $Z \leq 28$ incident on H, He, and C targets in terms of the number of incident nuclei and the different energies involved. Most of the earlier measurements, involving proton beams incident on heavier targets, for example, measured the cross sections for the production of individual radioactive isotope fragments. In a few cases this work was complete enough to obtain the individual charge changing cross sections by summing these isotopic cross sections. We mention here the work of Perron[5] using proton beams incident on Fe targets. The summed isotopic cross sections from this experiment are in good agreement with our elemental cross sections obtained from Fe beams (see data points plotted in Figs. 13 and 14).

With the advent of the Bevalac, the capacility to measure both elemental and isotopic cross sections increased dramatically. The work of Lindstrom *et al.*[6] and Westfall *et al.*[7] obtained elemental cross sections for ~2 GeV/nucleon C, O, and Fe nuclei that are in good agreement with our results (see data points plotted in Figs. 9, 10, and 13). More recently, Brechtmann and Heinrich[8] have studied the fragmentation of 720 MeV/nucleon ^{32}S in carbon and hydrogen targets and derived a set of elemental fragmentation cross sections directly comparable with ours measured at almost the same energy. For fragments with $\Delta Z = 1$–10 in carbon targets their cross sections differ from ours by an average ~7% with a maximum difference ~15%; for hydrogen targets the average elemental cross section difference is ~8% with a maximum difference ~25% (for carbon fragments). These differences are generally within the experimental errors of the two measurements. We should also mention here the extensive measurements of the elemental fragmentation of higher Z beam nuclei at the Bevalac by the high-energy astronomy observatory (HEAO) group (e.g., Binns *et al.*[9]) which, although they are in a different charge range, are comparable to ours in terms of technique and accuracy.

A. Relative cross sections in hydrogen and carbon targets

In this section we will compare the elemental cross sections obtained in carbon and hydrogen targets and examine the question of factorization. (A comparison of the elemental cross sections obtained by us in helium and hydrogen targets has been described separately, Ferrando *et al.*[10].) In this study we will examine the ratio, σ_C/σ_H, both as a function of energy for a given charge and at a constant energy as a function of Z_B. In Fig. 3 we show the ratio of the individual elemental cross sections obtained in carbon targets to those obtained in hydrogen targets, as a function of the charge change ΔZ for incident ^{56}Fe nuclei at ten different energies, from 330 to 1615 MeV/nucleon. Recall that Westfall *et al.*,[7] from a study of ^{56}Fe fragmentation at 1.88 GeV/nucleon in several targets, suggested that the individual elemental

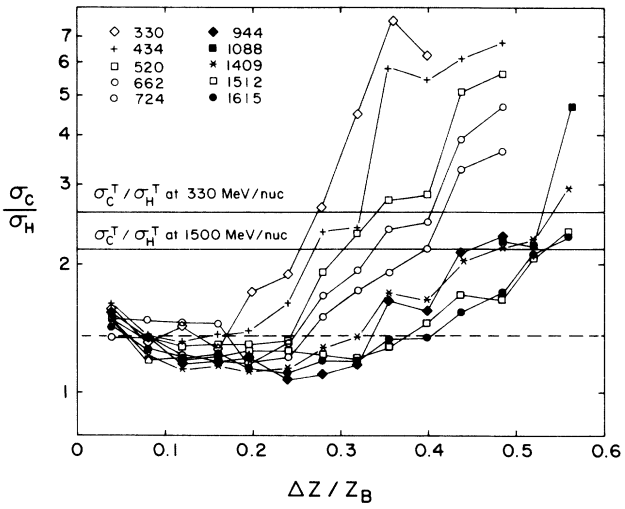

FIG. 3. Ratio of elemental cross sections in carbon and hydrogen targets for ^{56}Fe beams of various energies.

cross sections could be factored into a target factor γ_T, depending upon the target only, and a factor σ_B^i that depends on the beam and fragment—e.g.,

$$\sigma_{BT}^i = \gamma_T \sigma_B^i ,$$

where σ^i is the cross section of the ith fragment. They found that for fragments with $Z = 18$–24 the relative target factor between C and H targets was 1.36 ± 0.14. This factor is indicated by the dashed line in Fig. 3. Factorization of this type implies that the ratio of σ_C^i/σ_H^i should be constant as a function of $\Delta Z/Z_B$ for all energies where it holds. This is obviously not the case with the data shown in Fig. 3 which, however, shows several interesting trends. For the highest-energy points factorization is indeed approximately true, however, for $\Delta Z/Z_B \leq 0.5$ instead of being strictly constant, the ratio σ_C^i/σ_H^i actually goes through a minimum for $\Delta Z/Z_B \sim 0.25$ and then begins to increase rapidly for values of $\Delta Z/Z_B \gtrsim 0.5$. At lower energies the rapid increase in the σ_C^i/σ_H^i ratio moves to smaller and smaller values of $\Delta Z/Z_B$. In effect, the region where a simple factorization is approximately true covers a smaller and smaller range of $\Delta Z/Z_B$. This behavior of the individual elemental cross sections is consistent with the behavior of the total charge changing cross sections as well. The solid lines in Fig. 3 show the ratios of the total charge changing cross sections for carbon and hydrogen targets at two energies, as presented in paper I. This ratio increases as one goes to lower energies. This is consistent with the fact that the increase in the individual elemental σ_C^i/σ_H^i ratio moves to smaller values of $\Delta Z/Z_B$ as the energy decreases and the fact that the integrated effect of all of the elemental σ_C^i/σ_H^i ratios over all ΔZ, including those we do not measure, must produce the observed ratio of total cross sections for carbon and hydrogen targets.

This behavior may be examined in another way as illustrated by Fig. 4, which is a plot of the integrated frac-

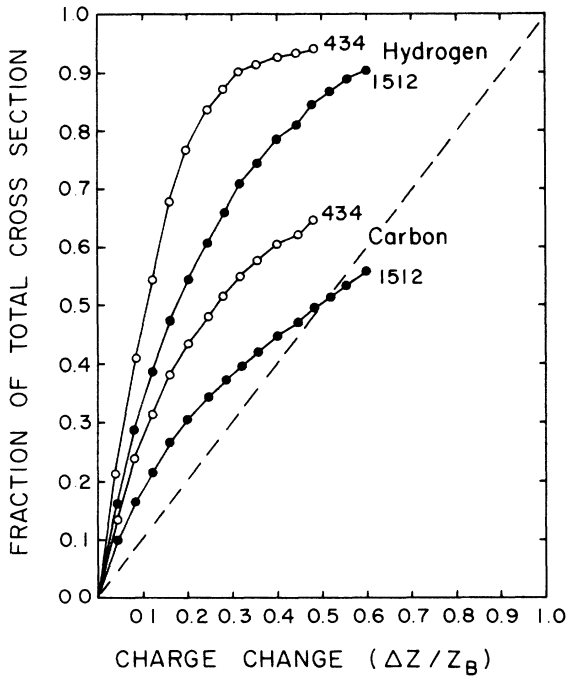

FIG. 4. The incremental sums of the elemental cross sections as a function of the charge charge for ^{56}Fe beams of 434 and 1512 MeV/nucleon incident on carbon and hydrogen targets.

tion of the total charge changing cross section given by the elemental cross sections, plotted as a function of the cumulative charge change.

This behavior may also be examined as a function of incident beam charge at a constant energy. In Fig. 5 we show the ratio, σ_C^i/σ_H^i, as a function of $\Delta Z/Z_B$ for an energy $\sim$600 MeV/nucleon for several beam nuclei. At this energy, for incident ^{56}Fe nuclei, the ratio is roughly constant for small values of $\Delta Z/Z_B$, rapidly increasing when $\Delta Z/Z_B > 0.3$. For lower Z beam nuclei at the same energy we observe that this ratio is roughly constant up to values of $\Delta Z/Z_B$ as large as 0.5. Also for different beam charges the ratio σ_C^i/σ_H^i for small ΔZ slowly increases with decreasing beam charge. This again is consistent with the behavior observed for the ratio of the total cross sections in carbon and hydrogen targets presented in paper I. This illustrates that for large $\Delta Z/Z_B$, even for low Z beams, the ratio σ_C^i/σ_H^i *must* increase rapidly as $\Delta Z/Z_B$ increases, in order that the integrated effect of these elemental ratios over all ΔZ must produce the observed ratio of the total charge changing cross sections in carbon and hydrogen targets, presented in paper I (shown in Fig. 5 as solid lines). This shows that the concept of factorization is a better approximation and extends to larger values of $\Delta Z/Z_B$ for lower Z beams.

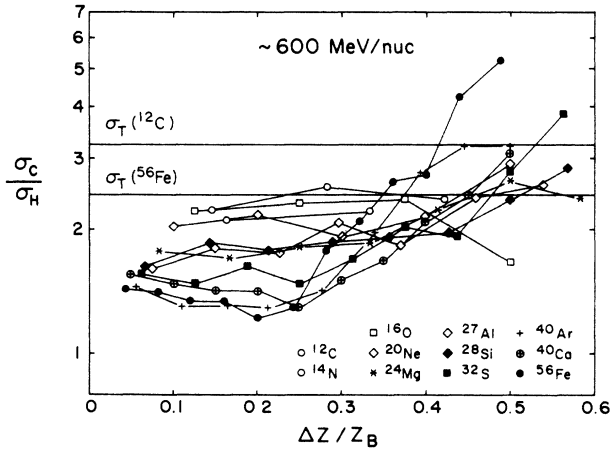

FIG. 5. Ratio of elemental cross sections in carbon and hydrogen targets at $\sim$600 MeV/nucleon for various beam charges.

Basically, this whole argument is closely related to the manner in which the individual elemental cross sections approach their high-energy asymptotic limit where the concept of factorization more closely applies. As we shall discuss later, the elemental cross sections for small charge change from low Z beams show very little energy dependence and have probably reached their asymptotic limit at $\sim$1500 MeV/nucleon. As the Z of the beam is increased, this energy dependence becomes more pronounced. For ^{56}Fe beams there is a very strong energy dependence of the elemental cross sections for small charge change and it is clear that they have not reached their asymptotic limit at $\sim$1500 MeV/nucleon.

B. Dependence of elemental cross sections on Z_f and $Z_B - Z_f$

Another very important systematic in our data has to do with a regular decrease at a constant energy in the elemental cross sections with increasing charge change, $Z_B - Z_f$. We find that this regular behavior can be parametrized very simply in terms of the fragment charge Z_f and the quantity $Z_B - Z_f$. This has extremely important implications for constructing an empirical formula to describe the cross sections, as well as having theoretical implications. Here we consider this behavior for hydrogen targets. We note that a similar behavior is observed by us for carbon targets, and also for higher Z beams, but in terms of Z_B rather than Z_f, by Binns *et al.*[9] Our data for each Z_f from 4 to 25 is shown in Figs. 6–8. For most Z_f the production from higher Z beams follows a simple exponential law in $Z_B - Z_f$:

$$\sigma_0 = \sigma_{Z_f} \exp \frac{-(Z_B - Z_f)}{\Delta_{Z_f}} \text{ mb} .$$

There are some exceptions to this behavior for neutron rich beam nuclei into adjacent elements, e.g., ^{11}B$\rightarrow$Be and ^{40}Ar$\rightarrow$Cl. Also for large values of $Z_B - Z_f$ some of the cross sections tend to be larger than predicted by a simple exponential behavior.

If we plot our data in the same manner as Binns *et al.*,[9] e.g., the cross section versus charge change for a *given* beam nucleus Z_B, we find large fluctuations from a regular decrease. The cross sections for the odd Z_f nu-

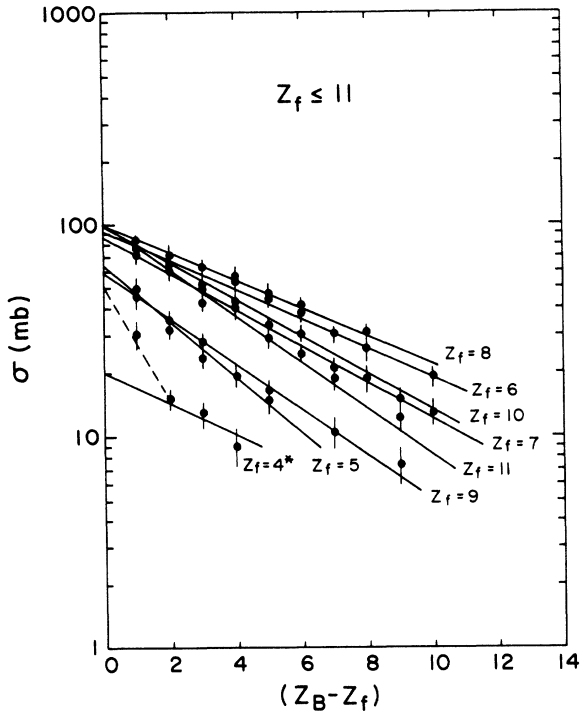

FIG. 6. Individual elemental cross sections as a function of ΔZ, the difference between the beam charge and the fragment charge, for $Z_f \leq 11$.

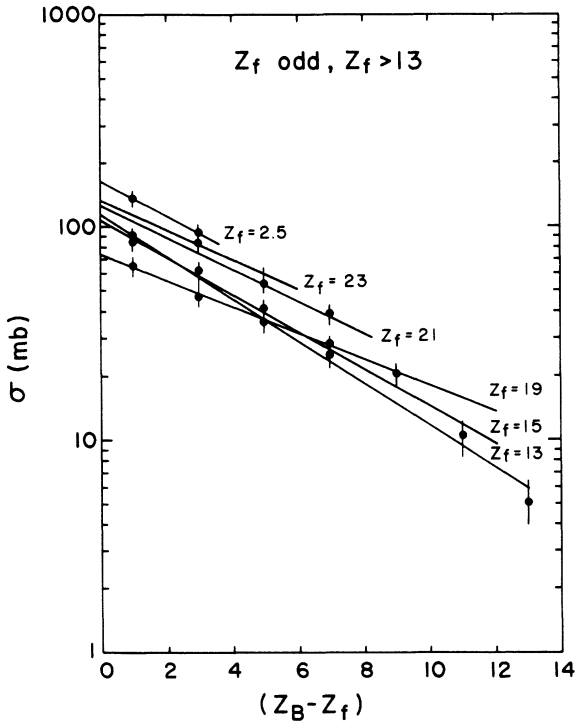

FIG. 8. Same as Fig. 6 except for odd $Z_f \geq 13$.

clei are generally much less than those for adjacent even Z_f nuclei. This strong odd-even effect of nuclear structure appears to be less important for the higher Z fragments from higher Z beams studied by Binns *et al.*[9]

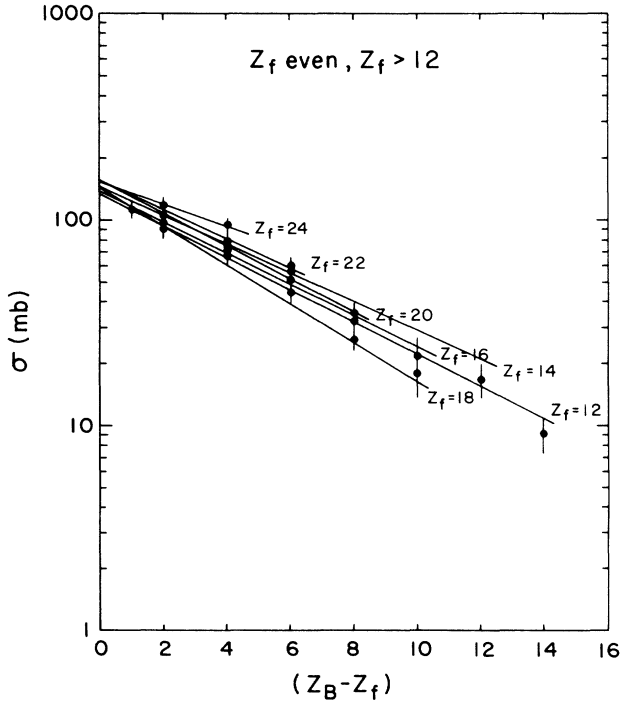

FIG. 7. Same as Fig. 6 except for even $Z_f > 12$.

In Table IV we summarize the values of σ_{Zf} and Δ_{Zf} determined over the range $1 \leq (Z_B - Z_f) \leq 12$ along with the reduced x^2 for each Z_f. It is seen that this simple formula is a remarkably good fit to the data over a wide

TABLE IV. Fitting parameters for production of $4 \leq Z_f \leq 25$ nuclei at 600 MeV/nucleon in hydrogen targets.

Z_f	σ_{Zf} (in mb)	Δ_{Zf}	x^2
25	161.4	5.7	0.21(2)
24	154.6	8.2	0.36(2)
23	135.7	6.2	0.25(2)
22	158.0	6.2	0.20(2)
21	126.6	5.9	0.93(2)
20	160.2	5.9	0.62(2)
19	74.8	6.9	0.38(3)
18	144.5	4.9	2.32(3)
17	140.1	4.5	1.97(3)
16	142.5	5.6	2.56(3)
15	112.5	4.9	2.87(4)
14	145.0	6.2	4.22(4)
13	112.0	4.3	1.84(5)
12	134.5	6.2	2.21(5)
11	102.5	4.1	4.55(5)
10	99.2	5.4	1.02(6)
9	59.2	3.1	2.72(7)
8	99.2	6.3	1.39(7)
7	86.6	4.8	2.24(6)
6	94.0	6.2	2.21(8)
5	61.2	3.9	3.75(5)
4	19.6	6.1	2.40(4)

range of $Z_B - Z_f$, subject to the exceptions noted earlier. A similar kind of exponential behavior was the basis for some of the initial semiempirical fits to the measurements of cross sections of individual isotopes produced by the spallation of heavy nuclei by protons, e.g., Rudstam.[11] Note that there are some strong odd-even effects in the parameter Δ_{Zf} for the lower Z fragment production. This trend also exists, although less strongly, in the values of the parameter σ_{Zf} for the lower Z fragments.

C. Energy dependence of cross sections

Finally we turn to the energy dependence of the elemental cross sections. Here again we concentrate on the cross sections for hydrogen targets since they are of most interest for cosmic-ray studies. The energy dependence of the cross sections is known to have a characteristic shape that can be related to the reaction mechanism. Such features as the reaction threshold at low energies, the slope of the excitation function as it rises, the energy at which it peaks (if there is a maximum), and the behavior as it approaches its high-energy asymptotic limit are all significant features. As the mass difference between the beam and product nuclide increases, it is known that the threshold energy increases and the peak energy also increases indicating the competition of various intranuclear reactions. The systematics of these energy dependences have never been studied in such great detail over this intermediate energy range, however,

We begin by examining the cross sections for lower Z beams, extending these studies to higher and higher Z beams up to ^{56}Fe. In Fig. 9 we show the measured cross sections as a function of energy for the B and Be fragments from ^{12}C nuclei incident on hydrogen targets. These cross sections are nearly independent of energy, but show a slight decrease below $\sim$1 GeV/nucleon. The agreement of our data with the data of Lindstrom *et al.*,[6] at 1.05 and 2.1 GeV/nucleon is excellent. The cross sections obtained by Fontes,[12] at 600 MeV/nucleon using a proton beam incident on a carbon target appear to be $\sim$30% higher than those we measure. These cross sections were based on ratios to the monitor reaction, $^{12}C \rightarrow {}^{7}Be$. Our isotopic data, to be discussed in paper III (Ref. 13), as well as that of Lindstrom *et al.*,[6] leads to a lower production of ^{7}Be in the energy range 0.4–2 GeV/nucleon for this reaction than the monitor reaction cross sections used by Fontes.[12] If his cross sections are corrected using this most recent data for the $^{12}C \rightarrow {}^{7}Be$ reaction, then his 600 MeV/nucleon points must be reduced by $\sim$30% as indicated in Fig. 9, and are now in good agreement with our cross section data.

The solid curves in Fig. 9 are the cross sections determined from the new empirical cross section formula we present in paper IV (Ref. 14). The dashed curves are from an earlier semiempirical formula developed by Tsao and Silberberg[3] that has been widely used in previous cosmic-ray propagation calculations. This earlier formula predicts cross sections up to 30% larger than we measure below $\sim$1 GeV/nucleon and appears to be strongly influenced by the earlier Fontes[12] measurements. This is a very important difference since the B/C ratio is generally used as a reference to determine the path length traversed by cosmic rays in the galaxy as a function of energy and since $\sim$70% of all the cosmic-ray B is produced by ^{12}C, this reaction is of considerable importance.

In Fig. 10 we show the measured cross sections for the fragments from ^{16}O nuclei of various energies incident on hydrogen targets. Here again there are only small changes in the cross sections as a function of energy, but a pattern that becomes more pronounced as one goes to higher Z beam nuclei is becoming apparent. For fragments with a small charge change ΔZ, e.g., N, a distinct energy dependence is observed with the cross section becoming slightly larger below $\sim$1 GeV/nucleon. For fragments with a larger charge change, e.g., Be, the cross section is significantly less below $\sim$1 GeV/nucleon, and for fragments with intermediate charge change the cross sections are almost energy independent. Presumably all

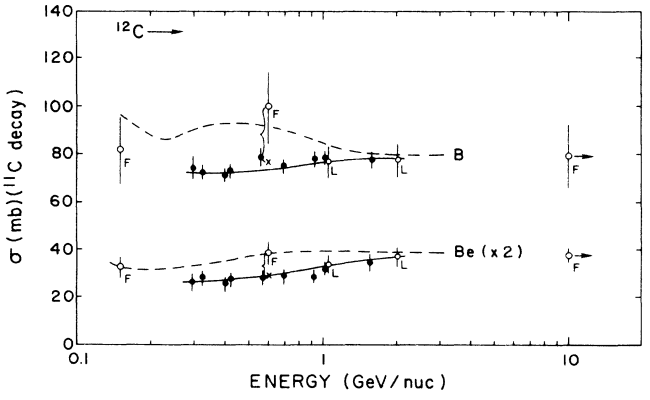

FIG. 9. Measured cross sections for B and Be fragments for ^{12}C beams incident on hydrogen targets. Solid lines are from the empirical cross section formula derived from this study—paper IV (Ref. 14). Dashed line is earlier semiempirical prediction of Tsao and Silberberg (Ref. 3). The symbol L refers to the data from Lindstrom *et al.* (Ref. 6); F refers to Fontes *et al.* (Ref. 12).

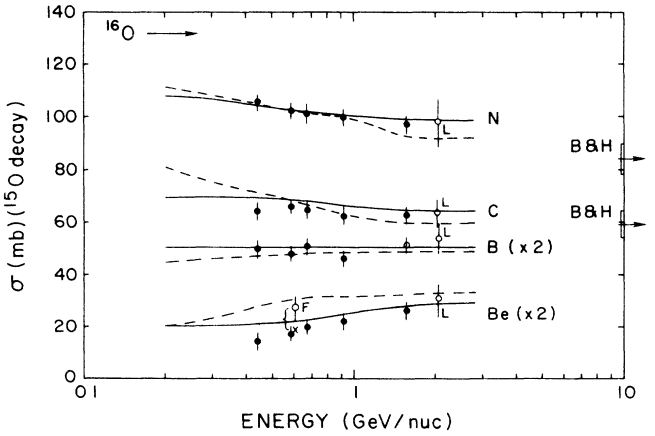

FIG. 10. Measured cross sections for fragments from ^{16}O beams of various energies incident on hydrogen targets. Lines and symbols same as Fig. 9. The symbol B and H refers to Brechtman and Heinrich (Ref. 15).

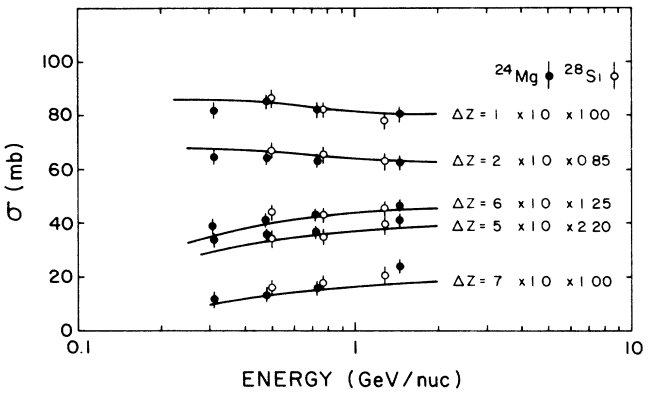

FIG. 11. Energy dependence of fragment cross section observed for ^{24}Mg and ^{28}Si beams incident on hydrogen targets. Solid lines are the predictions for ^{24}Mg fragments from the empirical cross section formula derived from this study—paper IV.

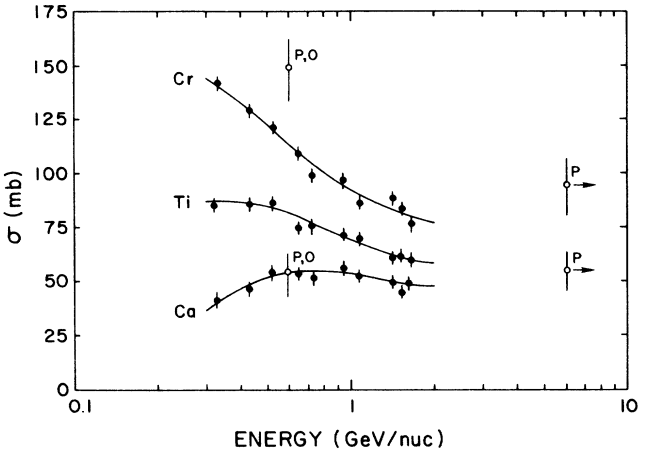

FIG. 13. Same as Fig. 12, except for Cr, Ti, and Ca fragments.

of the fragment cross sections of these lower Z beams have also reached their asymptotic high-energy values at 2 GeV/nucleon, however, we note that the rather unexpected cross sections measured by Brechtmann and Heinrich,[15] at ~200 GeV/nucleon, shown in Fig. 10, indicate that the cross sections for this reaction for C and N fragments may continue to decrease slowly even up to ~100 Gev/nucleon.

For intermediate Z beams we do not have as extensive a coverage in energy. In order to illustrate the energy dependence of secondary fragment production we have combined the data from ^{24}Mg beams measured at four energies and ^{28}Si beams measured at three energies. These data are shown in Fig. 11, for several values of the charge change. In the case of ^{28}Si, the data for the corresponding charge change is arbitrarily normalized to provide a fit to the ^{24}Mg data for the same charge change, since the secondary fragments in each case are different. The same pattern of the energy dependence of the hydrogen target cross sections for small charge change and for large charge change as observed for the ^{16}O beams is also observed for these intermediate Z beams. In this figure the solid lines refer to the predicted cross sections as a function of energy for fragments for a ^{24}Mg beam as obtained from our new cross section formula presented in paper IV (Ref. 14).

The most extensive information on the energy dependence of the fragment cross sections is available for ^{56}Fe beams, where data are available at nine energies between 330 and 1610 MeV/nucleon. Here also the largest and most complex energy dependence is observed. This data is shown in Figs. 12–14 for ten fragment charges between Cl and Mn, along with other experimental data. As before the solid lines are the predictions from our new cross-section formula. It should first be noted that many

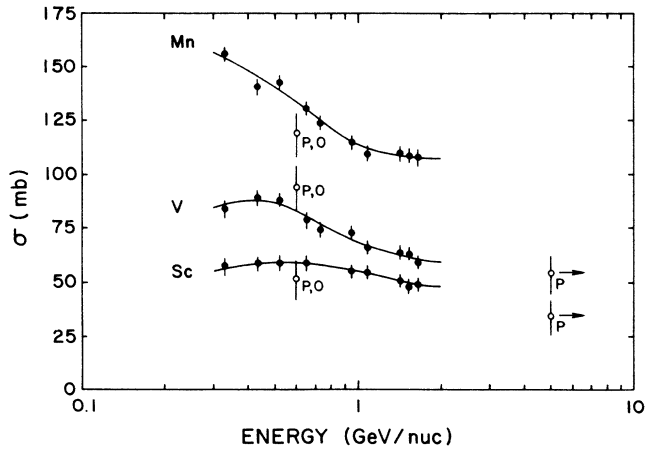

FIG. 12. Cross sections measured for Mn, V, and Sc fragments from ^{56}Fe interactions in hydrogen targets. Solid lines are from the empirical cross section formula derived from this study—paper IV. The symbols P and O, refer to the work of Perrion (Ref. 5) and Orth *et al.* (Ref. 16).

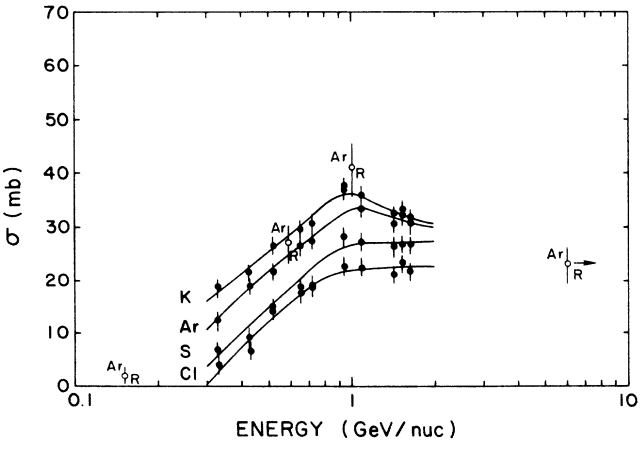

FIG. 14. Same as Fig. 12 except for K, Ar, Cl, and S fragments. The symbol R refers to the data from Regnier (Ref. 17).

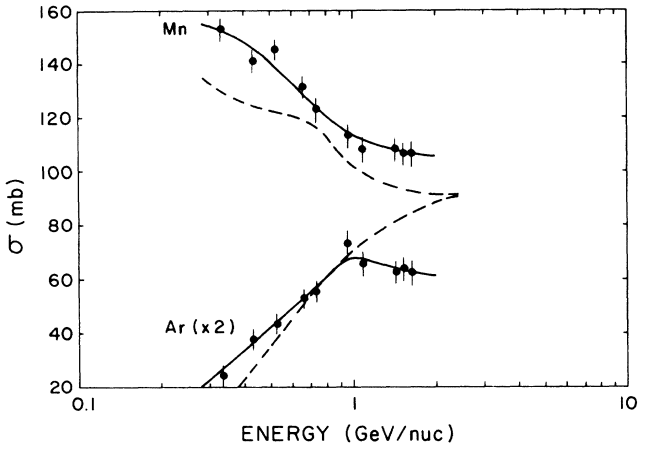

FIG. 15. Differences in fragment cross sections for $^{56}Fe \rightarrow Mn$ and $^{56}Fe \rightarrow Ar$ from this work (solid symbols and lines) and earlier predictions. Dashed lines are semiempirical cross sections from Tsao and Silberberg (Ref. 3).

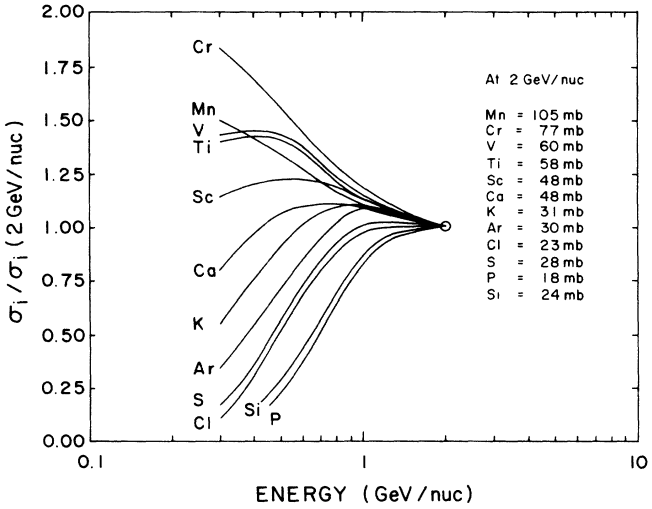

FIG. 16. Relative cross sections for production of secondary fragments from ^{56}Fe beams incident on hydrogen targets. All cross sections normalized at 2 GeV/nucleon beam, where the extrapolated cross section in mb is shown.

of these new measurements and predictions differ greatly from earlier predictions using the semiempirical formula of Tsao and Silberberg.[3] In Fig. 15 we illustrate these differences for two fragment charges of particular interest, Mn and Ar.

The energy dependence of these cross sections from ^{56}Fe shows a pattern with charge change that is similar to, but much enhanced, from that of the lower Z beam nuclei. For fragments with small charge change, the cross sections are much larger below ~ 1 GeV/nucleon, reaching a peak at a few hundred MeV/nucleon. For intermediate charge change ~ 5–6, the cross sections are more nearly independent of energy, but appear to decrease below a few hundred MeV/nucleon and to have a broad peak at ~ 1 GeV/nucleon. For larger charge change ~ 7–10, the decrease at lower energies is more pronounced and moves to higher energies as ΔZ increases. A maximum still appears in the cross sections at ~ 1 GeV/nucleon. For still larger charge change (not shown here) the elemental cross sections are still increasing toward their high-energy asymptotic values at the highest energies we measure.

In an attempt to display these energy dependent systematics more clearly we show Fig. 16, in which the elemental cross sections are all normalized to 1 at 2 GeV/nucleon. Except for the $\Delta Z = 1$ fragment Mn, and small even-odd effects for large ΔZ, the energy dependences scale systematically with increasing charge change. Note that the use of 2 GeV/nucleon as a reference does not imply that all of the cross sections have reached their high-energy asymptotic values at this energy. This is clearly not true for both small and large charge changes.

The parametrization of these energy dependent elemental cross sections as a function of Z_B and ΔZ will be addressed in the final paper of this series.[14]

[1]W. R. Weber, J. C. Kish, and D. A. Schrier, Phys. Rev. C **41**, 520 (1990), the preceding paper.
[2]W. R. Weber and D. A. Brautigam, Astrophys. J. **260**, 894 (1982).
[3]C. H. Tsao and R. Silberberg, Proc. 16th ICRC **2**, 202 (1979).
[4]W. R. Webber, Proc. 20th ICRC **8**, 65 (1987).
[5]C. Perron, Phys. Rev. C **14**, 1108 (1976).
[6]P. J. Lindstrom, D. E. Greiner, H. H. Heckman, B. Cork, and F. S. Bieser, Lawrence Berkeley Laboratory (LBL) Report No. 2650, 1975.
[7]G. D. Westfall, L. W. Wilson, P. J. Lindstrom, H. J. Crawford, D. E. Greiner, and H. H. Heckman, Phys. Rev. C **19**, 1309 (1979).
[8]C. Brechtmann and W. E. Heinrich, Proc. 20th ICRC **2**, 137 (1987).
[9]W. R. Binns, T. L. Garrad, M. H. Israel, M. P. Kertzmann, J. Klarmann, E. C. Stone, and C. J. Waddington, Phys. Rev. C **36**, 1870 (1987).
[10]P. Ferrando, W. R. Webber, P. Goret, J. C. Kish, D. A. Schrier, A. Soutoul, and O. Testard, Phys. Rev. C **37**, 1490 (1988).
[11]G. Rudstam, Z. Naturforsch. Teil A **21**, 1027 (1966).
[12]P. Fontes, C. Perron, J. Lestringuez, F. Yiou, and R. Bernas, Nucl. Phys. **165**, 405 (1974).
[13]W. R. Webber, J. C. Kish, and D. A. Schrier, Phys. Rev. C **41**, 547 (1990), the following paper.
[14]W. R. Webber, J. C. Kish, and D. A. Schrier, Phys. Rev. C **41**, 566 (1990), this issue.
[15]C. Brechtmann and W. E. Heinrich, Z. Phys. (in press).
[16]C. S. Orth, H. A. O'Brien, M. E. Schillaci, B. J. Dropesky, J. E. Cline, E. B. Nieschmidt, and R. L. Brodzinski, J. Inorg. Nucl. Chem. **38**, 13 (1976).
[17]S. Regnier, Phys. Rev. C **20**, 1517 (1979).